

Optical characterization of $\text{Cu}_2\text{ZnSnS}_4$ nanocrystals thin film

Z. Kışınışıci¹ · F. Özel² · Ö. F. Yüksel¹ · N. Tuğluoğlu³

Received: 22 February 2016 / Accepted: 30 May 2016 / Published online: 6 June 2016
© Springer Science+Business Media New York 2016

Abstract Synthesis of nanostructured powders of tetragonal $\text{Cu}_2\text{ZnSnS}_4$ (CZTS) nanocrystals was carried out based on the hot-injection process. High-quality CZTS thin films were prepared by spin coating method onto the Corning 1737 glass substrates. CZTS nanoparticles were characterized using X-ray diffraction (XRD), small-angle X-ray scattering (SAXS), transmission electron microscopy (TEM) and high resolution TEM. It is observed that a good quality CZTS film can be obtained by spin deposition at room temperature. The optical properties of the film were studied using UV–visible spectra between 300 and 1000 nm wavelength range. The direct optical band gap of the film evolved as 1.49 eV. This value is close to the ideal band gap for highest theoretical conversion efficiency of solar cell. The optical absorption coefficients of the film between 300 and 1000 nm are found to be about 2 and $7.6 \times 10^4 \text{ cm}^{-1}$, respectively. The optical dispersion parameters of the film were also determined by Wemple–DiDomenico single oscillator model.

1 Introduction

Thin-film chalcogen materials such as $\text{Cu}(\text{In,Ga})\text{Se}_2$ (CIGS) are used in solar cell application. CIGS are the highest performing thin film solar cells with efficiency of more than 20 % [1, 2]. However these material consists of uncommon and expensive materials as In and Ga. In recent years, the group I₂-II-IV-VI₄ quaternary semiconductors are used as an alternative to CdTe and $\text{Cu}(\text{In,Ga})\text{Se}_2$ (CIGS) since it is composed of abundant, inexpensive and nontoxic elements [3]. Among this group, $\text{Cu}_2\text{ZnSnS}_4$ (CZTS) is a promising material because of low cost, suitable optical band gap ($\sim 1.5 \text{ eV}$) [4, 5] and high absorption coefficient ($\sim 10^{4-6} \text{ cm}^{-1}$) [6, 7]. Moreover, CZTS are used as p-type semiconductors for absorber layers of thin films [8]. To synthesize CZTS films, several methods are used such as evaporation [9, 10], sputtering [11, 12], sol-gel method [13, 14], hot injection [15], pulsed laser deposition [16, 17]. Compared with the other techniques, spin coating method is cost-effective, easy to realize, safety, simplicity and suitable for mass production. Until now, the highest conversion efficiency of CZTS based thin film solar cells is reached to 12.6 % [18], this was fabricated by using a hydrazine-based solution via spin coating technology.

Kumar et al. [19] have reported the characterization and preparation of spray-deposited $\text{Cu}_2\text{ZnSnS}_4$ thin films. They concluded the optical band gap is found to lie between 1.40 and 1.45 eV and the average optical absorption coefficient is also found to be $4 \times 10^4 \text{ cm}^{-1}$. Patel et al. [20] have reported deposition of CZTS thin films by the Successive Ionic Layer Adsorption and Reaction (SILAR) technique using Chloride precursors at the room-temperature. They have reported that the band gap and absorption coefficient of this film are 1.5 eV and about 10^4 cm^{-1} in visible range,

✉ Ö. F. Yüksel
fyuksel@selcuk.edu.tr

¹ Department of Physics, Faculty of Science, Selçuk University, 42075 Konya, Turkey

² Department of Materials Science and Engineering, Faculty of Engineering, Karamanoğlu Mehmetbey University, 70200 Karaman, Turkey

³ Department of Energy Systems Engineering, Faculty of Engineering, Giresun University, 28200 Giresun, Turkey

respectively. Dhakal et al. [21] have reported the characterization of a CZTS thin film solar cell grown by sputtering method. They concluded the optical band gap and absorption coefficient are found to be 1.52 eV and $5 \times 10^4 \text{ cm}^{-1}$, respectively. Pawar et al. [22] have demonstrated a synthesis of single phase $\text{Cu}_2\text{ZnSnS}_4$ absorber prepared by the rapid thermal processing (RTP). They have concluded that the band gap energy of the CZTS absorber is found to be 1.50 eV. Tanaka et al. [23] have reported that CZTS thin films were prepared by sulfurizing precursors deposited by the sol-gel method. They have concluded that the band gap energy of the film was 1.49 eV at room temperature.

In present work, CZTS nanocrystals fabricated by hot-injection process were chosen as precursor and CZTS thin films were deposited by spin coating on Corning 1737 glass substrates. The goal of this study is to investigate the optical constants of the film such as optical band gap, absorption coefficient, refractive index and extraction coefficient constant. To our knowledge, no previous review focused on the optical dielectric and dispersion parameters of CZTS films in detail. To improve the optical parameters, more study is needed for CZTS film. The main goal of this study was to develop and determine these parameters according to Wemple-DiDomenico model.

2 Experimental Details

Copper (II) acetate ($\text{Cu}(\text{CO}_2\text{CH}_3)_2$), Zinc acetate ($(\text{CH}_3\text{CO}_2)_2\text{Zn}$), Sulfur powder, Ethanol were obtained from Sigma-Aldrich. Tin (II) acetate ($\text{Sn}(\text{OOCCH}_3)_2$) was from Alfa Aesar. Oleylamine - %80–90 (OLA), was obtained from Across Organic. Toluene and 2- Propanol were obtained from VWR.

Synthesis of nanostructured powders of tetragonal CZTS nanocrystals was carried out based on previously published hot-injection process by using metal salts and oleylamine precursors as starting materials and capping agent, respectively [24–26]. Typically; 1 mmol $\text{Cu}(\text{CO}_2\text{CH}_3)_2$, 0,5 mmol $(\text{CH}_3\text{CO}_2)_2\text{Zn}$, 0,5 mmol $\text{Sn}(\text{OOCCH}_3)_2$ and 20 mL OLA (80-90 %) were added to a 25 mL two-neck flask and heated to 280 °C under N_2 flow. Following the colors changes from blue to reddish brown, a solution of sulfur in oleylamine was added to above solution. Then, the temperature is increased to 280 °C and kept for 30 min by stirring. After cooling down to the room temperature, the resultants were participated and centrifuged. The final product was washed with ethanol and dried at 70 °C.

X-ray diffraction (XRD) and small-angle X-ray scattering (SAXS) patterns of CZTS nanoparticles were obtained on a Bruker (D8 Advance) with $\text{Cu-K}\alpha$ radiation source ($\lambda = 0.15,406 \text{ \AA}$). Zeiss Evo model scanning

electron microscope was used for analyzing of atomic percentage of elements. The microscopic images and selected area electron diffraction pattern (SAED) of samples were recorded by a transmission electron microscope (TEM, JEOL JEM-2100).

Before making thin film, glass was chemically cleaned by acetone, ethanol and pure water respectively with ultrasonic cleaning and then in UV-Ozone cleaner for 30 min and finally dried in nitrogen. Prepared CZTS nanocrystalline compound semiconductor was carried on a glass by spin coating method. Spin coating was performed at 1500 rpm spin speed for 60 s. The thickness of $\text{Cu}_2\text{ZnSnS}_4$ (CZTS) nanocrystalline thin film was measured 70 nm by using profilometer Veeco Dektak 150. Optical properties of the prepared nano particle based CZTS thin film were characterized by a Jasco model V-670 UV/VIS/NIR spectrophotometer. Transmission and reflection spectra of film were performed between 300 and 1000 nm wavelength range. The room temperature Raman spectra of nanocrystals was recorded Renishaw invia confocal-raman spectrometer.

3 Results and discussion

CZTS nanoparticles have been analyzed by using X-Ray Diffractometer for better understanding of crystalline structure. X-ray diffraction (XRD) pattern of colloidal CZTS nanocrystals is given in Fig. 1a. Characteristic peaks for nanocrystals are clearly observed on XRD patterns. We have to emphasize that, XRD peaks indicate two main crystalline structures as kesterite and stannite. Both structures are described by tetragonal unit cell. Since their same crystal structure, it is difficult to separate these structures from diffraction peaks. However, kesterite phase is more stable than stannite phase as reported many times in literature [15, 27]. The as-synthesized CZTS nanocrystals showed three intensive XRD peaks centered at $2\theta = 28.3^\circ$, 46.75° , 55.2° , 67.7° and 74.9° corresponding planes to (112), (220), (312), (008) and (332), respectively. As well known, XRD peaks are broadened by decreasing the particle size (Fig. 1a). The sample of nanocrystals shows broad diffraction peaks and this broad peaks are due to small size of the CZTS nanocrystals. The average particle size of the nanocrystals was calculated from the [112] diffraction peaks at 28.3° by using Debye-Sherrer equation as 18 nm, which is also confirmed by SAXS (Fig. 1b) and TEM analysis.

The structure and phase purity of the CZTS nanocrystals were investigated by using Raman analysis. The Raman spectra of CZTS nanocrystals is presented in Fig. 1c. The characteristic peak of CZTS is clearly observed on

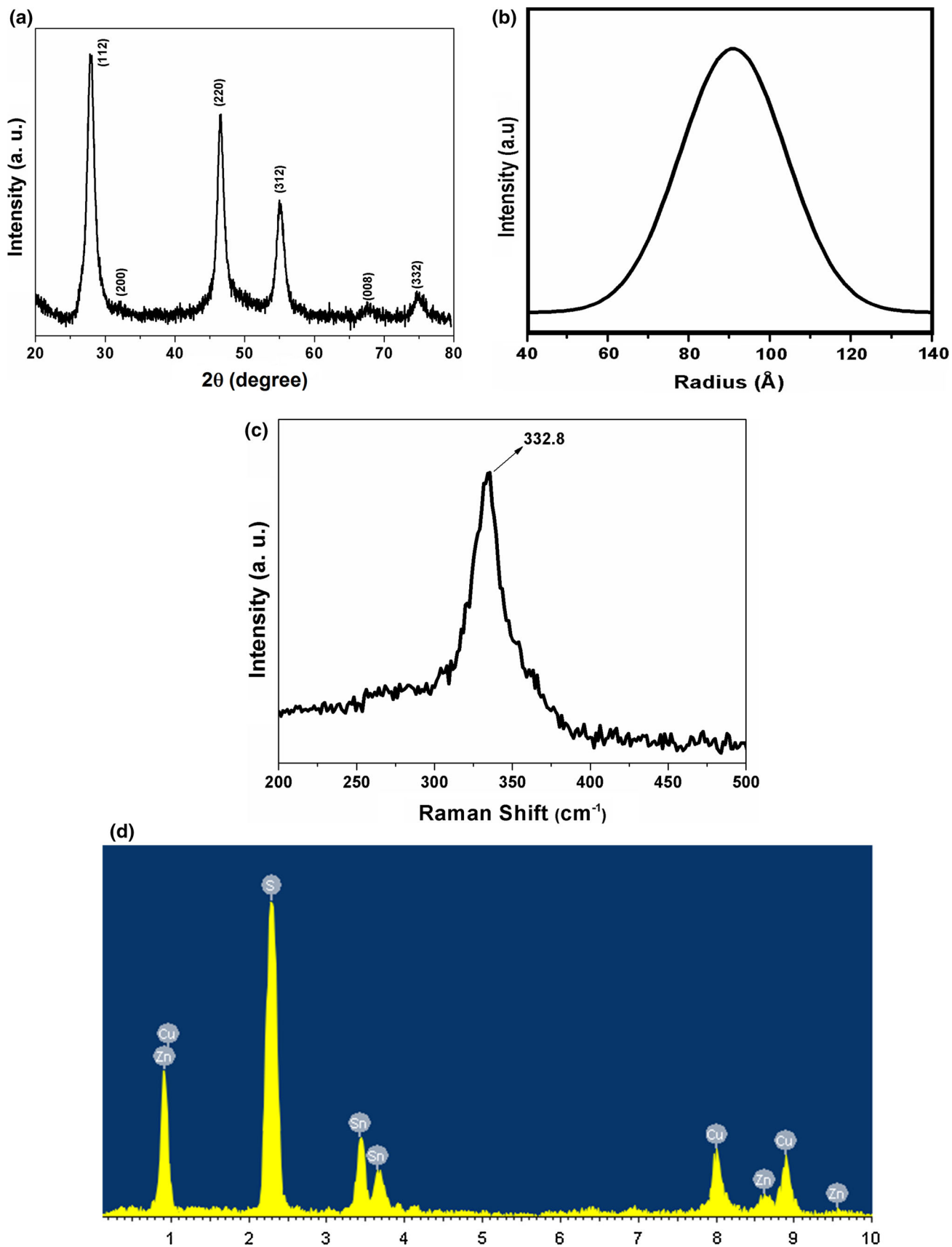


Fig. 1 **a** XRD pattern, **b** SAXS, **c** Raman spectra, and **d** EDS spectrum results of CZTS nanocrystals

spectrum. A Raman peak at 332.8 cm^{-1} corresponded to the A_1 mode of CZTS [28]. This value is in good agreement with the value obtained by Arora [29]. Compared to the standard peak at 338 cm^{-1} of the bulk CZTS materials, it is slightly shifted from the strong peak due to the dispersion of the phonon momentum [30]. Also there is no significant indication of phase separation for Sn_2S_3 at 304 cm^{-1} , Cu_2SnS_3 at 318 cm^{-1} , ZnS at 355 cm^{-1} , and Cu_{2-x}S at 475 cm^{-1} . Since no other crystalline forms were observed in the Raman spectrum, we strongly suggested that the structure of the CZTS samples shows high purity and crystallinity. Furthermore, the broadening of the Raman peak is seen for nanocrystals owing to the phonon confinement [31, 32], which is consistent with the XRD pattern.

Energy-dispersive X-ray spectroscopy (EDS) was performed to examine the overall homogeneity and composition of CZTS as an example of the synthesized nanocrystals. The EDS spectrum of CZTS nanocrystals is presented in Fig. 1d. As seen in Fig. 1d, the values of elemental composition of the nano particle based CZTS thin film are 25.17, 12.05, 12.87, and 49.91 for copper (Cu), zinc (Zn), tin (Sn), and sulfur (S), respectively. The Zn/Sn, Cu/Sn, and Cu/(Zn + Sn) ratios calculated in our film are estimated as 0.94, 1.96, and 1.01, respectively. The Cu/(Zn + Sn) and Zn/Sn ratios are desired in the vicinity of 0.8 and 1.2, respectively [33]. Furthermore, Dhakal et al. [21] have reported that the Cu/(Zn + Sn), Zn/Sn, and Cu/Sn ratios were 0.79, 1.58, and 2.03, respectively. Moreover, the average elemental composition ratio of CZTS nanocrystals were found as $\text{Cu}_2\text{Zn}_1\text{Sn}_1\text{S}_4$ which is revealed that CZTS sample close to the ideal composition.

Figure 2 shows transmission electron microscopy (TEM) images and selected area diffraction (SAED) patterns of the as synthesized CZTS nanocrystals. As can be clearly seen from Fig. 2a, most of the nanocrystals are spherical and the nanocrystals have an average size of 18 nm. The standard

deviation of nanocrystals was measured $\sim 2\text{ nm}$. To further study crystallinity and confirm the structure of the fabricated nanofibers, HR-TEM analysis was carried out (Fig. 2b). All of the lattice fingers of the synthesized CZTS nanocrystals revealed the highly crystalline nature. Moreover, interplanar spacing of 3.1 \AA was measured and attributed to the (112) crystallographic planes. Figure 2c shows the SAED pattern of the nanocrystals, in which three main diffraction rings correspond to (112), (220) and (312) planes of polycrystalline CZTS nanocrystals with tetragonal structure [15, 26, 27, 34]. As shown in inset figures, the diffraction rings are discontinuous and consist of sharp spots, which indicate that the nanocrystals are well crystallized. These results are consistent with the XRD data. Furthermore, XRD, SAXS, Raman spectra, EDS and TEM results correspond to the CZTS nanoparticles before spin deposition.

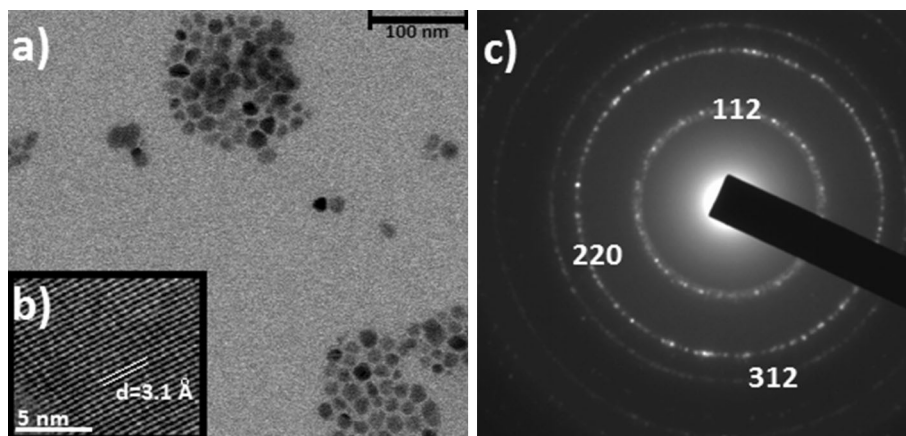
To determine optical parameters of nano particle based CZTS thin film, transmission and reflection spectra of the film were performed between 300 and 1000 nm wavelength range. The measured transmission (T) and reflection spectra (R) of nano particle based CZTS thin film are depicted in Fig. 3. According to Fig. 3, while transmission of sample has 50–65 % values in the visible wavelength region, it is about 65–70 % and approximately constant in the near infrared wavelength region. On the other hand, Fig. 3 shows that the thin film has a low reflectivity (~ 7 –12 %) in the visible and near infrared region.

The absorption coefficient has been calculated from the experimental data of transmission T and reflection R using the relation [19, 21, 35]:

$$\alpha = \frac{1}{d} \ln \left[\frac{(1-R)^2}{T} \right] \quad (1)$$

where d is the thickness of film. Figure 4a shows the variation of absorption coefficient of films with the

Fig. 2 a TEM b HRTEM images and c SAED pattern of nanocrystals



wavelength. The values of the absorption coefficient of the nano particle based CZTS film were found to be about $4\text{--}7 \times 10^4 \text{ cm}^{-1}$ in visible region. The figure shows that absorption coefficient is higher than 10^4 cm^{-1} measured in the VIS–NIR region, which is consistent with those reported in earlier published results [19, 21, 35] and therefore, the nano particle based CZTS film is considered as a suitable material for photovoltaic solar energy conversion. The higher absorption coefficient in lower energy region (longer wavelength region) is caused by defects in crystal structure. Many articles in the literature have high absorption coefficient for $\text{Cu}_2\text{ZnSnS}_4$ (CZTS) thin films. Dhakal et al. [21] have prepared $\text{Cu}_2\text{ZnSnS}_4$ (CZTS) thin films by sputtering method. They reported that the absorption coefficient calculated using the transmittance

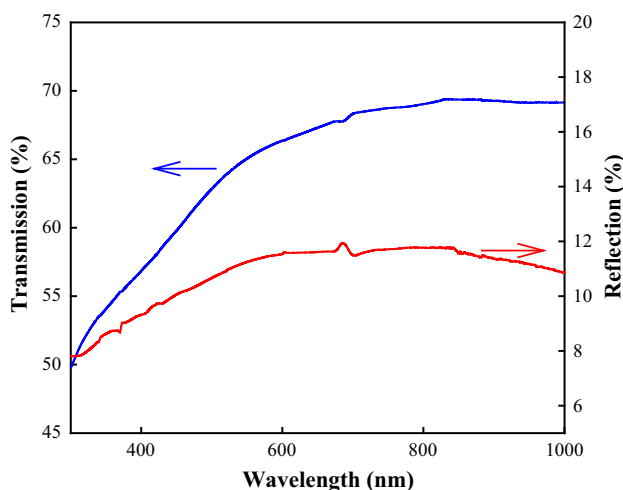


Fig. 3 Spectral variation of transmission and reflection of thin film

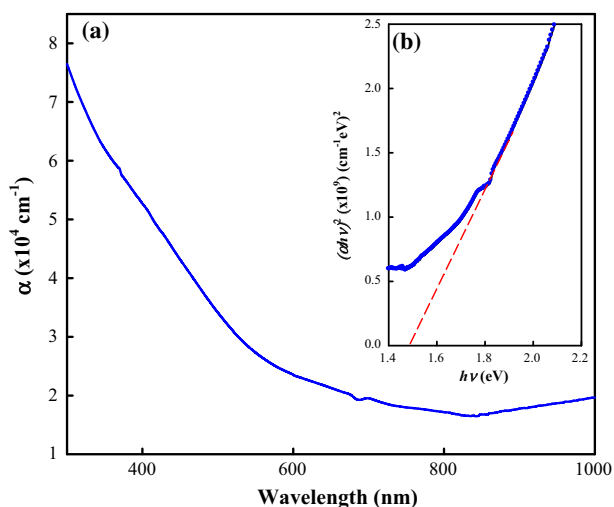


Fig. 4 **a** Plot of α versus λ of thin film and **b** Plot of $(\alpha hv)^2$ versus (hv) of thin film

and reflectance data was higher than $5 \times 10^4 \text{ cm}^{-1}$ in most of the visible region. Tanaka et al. [23] have prepared solutions for $\text{Cu}_2\text{ZnSnS}_4$ (CZTS) precursors by sol–gel method and deposited CZTS thin films by spin coating method by means of the solutions on soda-lime glass substrates. The absorption coefficient in the visible region was larger than 10^4 cm^{-1} , $2.7 \times 10^4 \text{ cm}^{-1}$ at 700 nm (1.77 eV) and $7.4 \times 10^4 \text{ cm}^{-1}$ at 400 nm (3.1 eV), and hence, CZTS is suitable material for thin-film solar cell. The fundamental absorption is characterized by a high absorption coefficient region ($\alpha > 10^4 \text{ cm}^{-1}$). It corresponds to electron excitation from the valence band to conduction band. The absorption coefficient reported in Refs. [36, 37] was $10^4\text{--}10^5 \text{ cm}^{-1}$ in visible region. Guan et al. [31] have prepared $\text{Cu}_2\text{ZnSnS}_4$ (CZTS) thin films on glass substrates by the solvothermal method. They reported that the absorption coefficient in the visible region was larger than 10^4 cm^{-1} , $2.0 \times 10^4 \text{ cm}^{-1}$ at 700 nm (1.77 eV) and $7.0 \times 10^4 \text{ cm}^{-1}$ at 400 nm (3.0 eV). Muhunthan et al. [38] have prepared $\text{Cu}_2\text{ZnSnS}_4$ (CZTS) thin films by the reactive co-sputtering process. They reported that the absorption coefficient in the visible region was larger than 10^4 cm^{-1} , $6.0 \times 10^4 \text{ cm}^{-1}$ at 700 nm (1.77 eV) and $6.5 \times 10^4 \text{ cm}^{-1}$ at 400 nm (3.0 eV). These band gap energies and absorption coefficients are comparable with our results.

To determine the band gap energy of materials, in common, the variation of αhv with $(hv - E_g)^n$ is investigated, where hv is the photon energy, E_g is the optical band gap, and n is either $1/2$ for indirect transition or 2 for direct transition. Therefore, we have plotted the graph of $(\alpha hv)^2$ versus hv to determine the direct optical band gap energy of nano particle based CZTS, as shown in inset of Fig. 4b. As seen in inset of Fig. 4b, the linear region is obtained. The optical band gap (E_g) is calculated by extrapolating this linear region of the plot $(\alpha hv)^2$ versus photon energy (hv). The optical band gap energy is found to be about 1.49 eV for our nano particle based CZTS thin film, which is in good agreement with the reported values [20, 21, 39]. The direct band gap energy of the deposited nano particle based CZTS thin films are in the solar energy range. Furthermore, Kumar et al. [19] are found that the optical band gap of high quality CZTS films prepared at different substrate temperatures lie between 1.40 and 1.45 eV. Dhakal et al. [21] have prepared $\text{Cu}_2\text{ZnSnS}_4$ (CZTS) thin films by sputtering method. They reported that the band gap derived using a Tauc plot was 1.52 eV. Tanaka et al. [23] reported that the band gap of the film was 1.49 eV for high quality CZTS thin films. The band gap energy reported in Refs. [36, 37] was 1.45 and 1.51 eV, respectively. Furthermore, Guan et al. [31] have prepared $\text{Cu}_2\text{ZnSnS}_4$ (CZTS) thin films on glass substrates by the solvothermal method. They reported that the band gap of the CZTS film was 1.50 eV.

Muhunthan et al. [38] have prepared Cu₂ZnSnS₄ (CZTS) thin films by the reactive co-sputtering process. They reported that the band gap of the film was 1.47 eV.

The refractive index n contains an imaginary part and is written as [19, 40]

$$n = n - ik. \tag{2}$$

Imaginary part of refractive index, the extinction coefficient k , can be calculated from the absorption coefficient α using the relation of $k = \alpha\lambda/4\pi$. Figure 5 shows the change of the extinction coefficient and refractive index of nano particle based CZTS thin film with the wavelength.

Now we can calculate the refractive index (n) of thin film from the reflection R and the extinction coefficient k values using the following relation [19–21, 39, 40]

$$n = \left(\frac{1 + R}{1 - R} \right) + \sqrt{\frac{4R}{(1 - R)^2} - k^2} \tag{3}$$

As seen from Fig. 5, the extinction coefficient has the values changed between 0.19 and 0.22 % until 600 nm, then k increase monotonically with increasing wavelength at higher wavelength regions. On the other hand, the calculated refractive index was found to be in the range of 1.7–2.

One of the main optical characteristics of any material is the complex dielectric function. The real (ϵ_1) and imaginary (ϵ_2) parts of the dielectric function are dependent on its refractive index and extinction coefficient and calculated from the following relations [39, 40]:

$$\epsilon_1 = n^2 - k^2 \tag{4}$$

$$\epsilon_2 = 2nk. \tag{5}$$

The variation of ϵ_1 and ϵ_2 with wavelength are presented in Fig. 6, respectively. As seen in Fig. 6, the ϵ_1 increases from 3.1 to 3.7 in visible region and also remains at a constant value between 600 and 800 nm and then decreases

towards 3.5 value after 800 nm. Furthermore, the ϵ_2 increases from 0.79 to 0.81 in visible region and then increases towards 1.1 value after 800 nm. The plot of the real part of the dielectric function in Fig. 6 is also quite similar to the n graph of the film.

The dispersion of the refractive index of any material is analysed using the single oscillator model proposed by Wemple and DiDomenico [40–42].

$$n^2 = 1 + \frac{E_d E_o}{E_o^2 - (hv)^2} \tag{6}$$

By plotting $1/(n^2-1)$ against $(hv)^2$, a straight linear region is obtained (Fig. 7). E_o the single oscillator energy and E_d the dispersion energy are determined by this linear region. The intercept of the linear curve at vertical axes gives E_o/E_d and its slope the value of $1/E_o E_d$. The

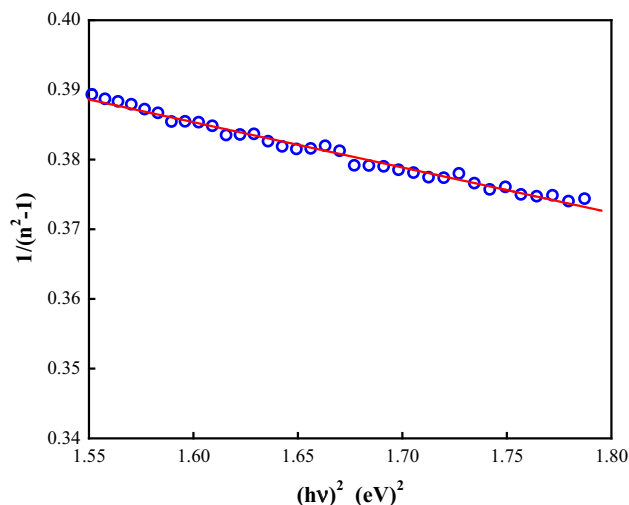


Fig. 7 Plot of $1/(n^2-1)$ against $(hv)^2$ of thin film

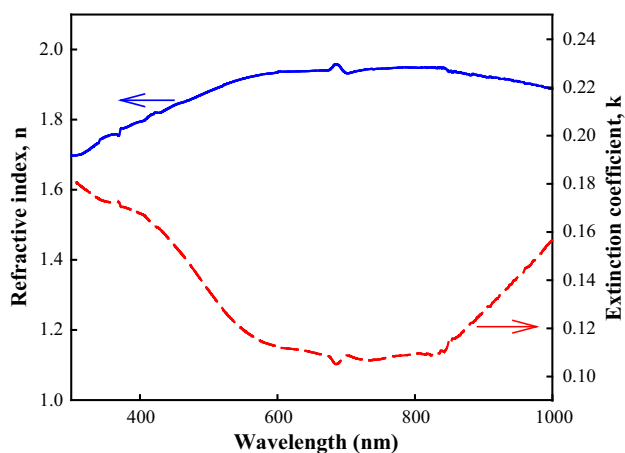


Fig. 5 Plot of n and k versus λ of thin film

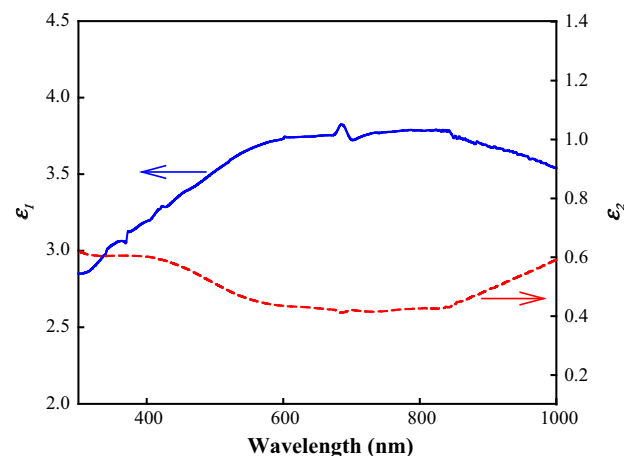


Fig. 6 The real and imaginary parts of dielectric constant of thin film

calculated E_o and E_d were found as 3.765 and 7694 eV, respectively. It seems that, the single oscillator energy E_o obeys an empirical relation such as $E_o = 2.5E_g$. The static refractive index, n_o can be calculated by $n_o = \sqrt{1 + \frac{E_d}{E_o}}$ as 1.74.

The M_{-1} and M_{-3} moment values of the optical spectra were calculated from the E_o and E_d , using following relationships [40–43]:

$$E_o^2 = \frac{M_{-1}}{M_{-3}} \quad (7)$$

$$E_d^2 = \frac{M_{-1}^3}{M_{-3}} \quad (8)$$

The calculated moment values were found as $M_{-1} = 2.04 \text{ eV}^{-2}$ and $M_{-3} = 0.295 \text{ eV}^{-2}$.

4 Conclusions

In this work, the I₂-II-IV-VI₄ quaternary compound Cu₂ZnSnS₄ (CZTS) nanocrystalline thin film was produced by hot-injection method. CZTS film with nanoparticle was prepared by spin coating method on Corning 1737 glass. Surface morphological, optical and structural properties of nano particle based CZTS thin films have been investigated in detail. The XRD analysis confirmed that the CZTS films exhibit the kesterite structure with preferential orientation along the (112) direction. The as-synthesized CZTS nanocrystals showed three intensive XRD peaks centered at $2\theta = 28.3^\circ$, 46.75° , 55.2° , 67.7° and 74.9° corresponding planes to (112), (220), (312), (008) and (332), respectively. The optical constants were calculated by means of transmission and reflection measurements. The values of the absorption coefficient of the film were found to be about $4\text{--}7 \times 10^4 \text{ cm}^{-1}$ in visible region. The direct optical band gap of this film is 1.49 eV, which is very close to the optimum value of the band gap required for the absorber material in thin film solar cell. According to the wavelength dependence of and of the nano particle based CZTS film, the refractive index (n) values vary from 1.78 to 1.97 in visible region. The extinction coefficient (k) values vary from 0.21 to 0.19 in visible region and increases rapidly toward 0.29 value in the ranging of 800–1000 nm. In addition, the dispersion of the refractive index is discussed in terms of the Wemple–DiDomenico single oscillator model. The values obtained for E_o , E_d , and n_o parameters are 3.765, 7.694, and 1.74 eV, respectively.

Acknowledgments This work is supported by Selçuk University BAP office with the research Project Number 14101020.

References

1. P. Jackson, D. Hariskos, E. Lotter, S. Paetel, R. Wuerz, R. Menner, W. Wischmann, M. Powalla, *Prog. Photovolt.* **19**, 894 (2011)
2. P. Jackson, D. Hariskos, R. Wuerz, W. Wischmann, M. Powalla, *Phys. Status Solidi RRL* **8**, 219 (2014)
3. H. Katagiri, K. Jimbo, W.S. Maw, K. Oishi, M. Yamazaki, H. Araki et al., *Thin Solid Films* **517**, 2455 (2009)
4. W. Liu, B. Guo, C. Mak, A. Li, X. Wu, F. Zhang, *Thin Solid Films* **535**, 39 (2013)
5. X. Jiang, L.X. Shao, J. Zhang, D. Li, W. Xie, C.W. Zou, J.M. Chen, *Surf. Coat. Technol.* **228**, S408 (2013)
6. K. Ito, T. Nakazawa, *J. Appl. Phys.* **27**, 2094 (1988)
7. D.B. Mitzi, O. Gunawan, T.K. Todorov, K. Wang, S. Guha, *Sol. Energy Mater. Sol. Cells* **95**, 1421 (2011)
8. S. Thiruvenkadam, D. Jovina, A.L. Rajesh, *Sol. Energy* **106**, 166 (2014)
9. T. Tanaka, D. Kawasaki, M. Nishio, Q. Guo, H. Ogawa, *Phys. Status Solidi C* **3**, 2844 (2006)
10. B. Shin, O. Gunawan, Y. Zhu, N.A. Bojarczuk, S.J. Chey, S. Guha, *Prog. Photovolt.: Res. Appl.* **21**, 72 (2013)
11. S.W. Shin, S.M. Pawar, C.Y. Park, J.H. Yun, J.H. Moon, J.H. Kim, J.Y. Lee, *Sol. Energy Mater. Sol. Cells* **95**, 3202 (2011)
12. K. Jimbo, R. Kimura, T. Kamimura, S. Yamada, W.S. Maw, H. Araki, K. Oishi, H. Katagiri, *Thin Solid Films* **515**, 5997 (2007)
13. Y. Miyamoto, K. Tanaka, M. Oonuki, N. Moritake, H. Uchiki, *Jpn. J. Appl. Phys.* **47**, 596 (2008)
14. Z.H. Su, K.W. Sun, Z.L. Han, H.T. Cui, F.Y. Liu, Y.Q. Lai et al., *J. Mater. Chem. A* **2**, 500 (2014)
15. Q. Guo, H.W. Hillhouse, R. Agrawal, *J. Am. Chem. Soc.* **131**, 11672 (2009)
16. K. Moriya, K. Tanaka, H. Uchiki, *Jpn. J. Appl. Phys.* **46**, 5780 (2007)
17. S.M. Pawar, A.V. Moholkar, I.K. Kim, S.W. Shin, J.H. Moon, J.I. Rhee, J.H. Kim, *Curr. Appl. Phys.* **10**, 565 (2010)
18. W. Wang, M.T. Winkler, O. Gunawan, T. Gokmen, T.K. Todorov, Y. Zhu, D.B. Mitzi, *Adv. Energy Mater.* **4**, 1301465 (2014)
19. Y.B.K. Kumar, G.S. Babu, P.U. Bhaskar, V.S. Raja, *Sol. Energy Mater. Sol. Cells* **93**, 1230 (2009)
20. K. Patel, D.V. Shah, V. Kheraj, *J. Alloys Compd.* **622**, 942 (2015)
21. T.P. Dhakal, C.Y. Peng, R.R. Tobias, R. Dasharathy, C.R. Westgate, *Sol. Energy* **100**, 23 (2014)
22. S.M. Pawar, A.I. Inamdar, B.S. Pawar, K.V. Gurav, S.W. Shin, X. Yanjun, S.S. Kolekar, J.H. Lee, J.H. Kim, H. Im, *Mater. Lett.* **118**, 76 (2014)
23. K. Tanaka, N. Moritake, H. Uchiki, *Sol. Energy Mater. Sol. Cells* **91**, 1199 (2007)
24. S.C. Riha, B.A. Parkinson, A.L. Prieto, *J. Am. Chem. Soc.* **131**, 12054 (2009)
25. A. Shavel, J. Arbiol, A. Cabot, *J. Am. Chem. Soc.* **132**, 4514 (2010)
26. M. Kuş, F. Özel, S. Büyükçelebi, A. Aljabour, A. Erdoğan, M. Ersöz, N.S. Sariçiftci, *Opt. Mater.* **39**, 103 (2015)
27. F. Özel, M. Kuş, A. Yar, E. Arkan, M.Z. Yiğit, A. Aljabour, S. Büyükçelebi, C. Tozlu, M. Ersöz, *Mater. Lett.* **140**, 23 (2015)
28. X. Zhai, H. Jia, Y. Zhang, Y. Lei, J. Wei, Y. Gao, J. Chu, W. He, J.J. Yinc, Z. Zheng, *Cryst. Eng. Comm.* **16**, 6244 (2014)
29. L. Arora, P. Gupta, N. Chhikara, O.P. Singh, N. Muhunthan, V.N. Singh et al., *Appl. Nanosci.* **5**, 163 (2015)
30. P.K. Sarswat, M.L. Free, *J. Cryst. Growth* **372**, 87 (2013)
31. H. Guan, H. Hou, F. Yu, L. Li, *Mater. Lett.* **159**, 200 (2015)
32. A. Singh, H. Geaney, F. Laffir, K.M. Ryan, *J. Am. Chem. Soc.* **134**, 2910 (2012)

33. Q. Guo, G.M. Ford, W. Yang, B.C. Walker, E.A. Stach, H.W. Hillhouse, R. Agrawal, *J. Am. Chem. Soc.* **132**, 17384 (2010)
34. S.S. Mali, P.S. Patil, C.K. Hong, *A.C.S. Appl. Mater. Interfaces* **6**, 1688 (2014)
35. C.P. Chan, H. Lam, C. Surya, *Sol. Energy Mater. Sol. Cells* **94**, 207 (2010)
36. J. Seol, S. Lee, J. Lee, H. Nam, K. Kim, *Sol. Energy Mater. Sol. Cells* **75**, 155 (2003)
37. K. Ito, T. Nakazawa, *Jpn. J. Appl. Phys.* **27**, 2094 (1988)
38. N. Muhunthan, O.P. Singh, V. Toutam, V.N. Singh, *Mater. Res. Bull.* **70**, 373 (2015)
39. J.J. Scragg, P.J. Dale, L.M. Peter, *Thin Solid Films* **517**, 2481 (2009)
40. M. Yıldırım, F. Özel, N. Tuğluoğlu, Ö.F. Yüksel, M. Kuş, *J. Alloys Compd.* **666**, 144 (2016)
41. Z. Kışnişci, Ö.F. Yüksel, M. Kuş, *Synth. Met.* **194**, 193 (2014)
42. M. DiDomenico, S.H. Wemple, *J. Appl. Phys.* **40**, 720 (1969)
43. S.H. Wemple, M. DiDomenico, *Phy. Rev B.* **3**, 1338 (1971)